Paper
02455

CORROSION2002

PASSIVE FILM CHEMISTRY on 316L STAINLESS STEEL ENNOBLED BY BIOMINERALIZED MANGANESE

Nurdan Yurt
Center for Biofilm Engineering and Chemical Engineering
Montana State University, EPS 366, Bozeman, MT 59717

Recep Avci
Department of Physics, Montana State University, EPS 254, Bozeman, MT 59717

Zbigniew Lewandowski*

Center for Biofilm Engineering and Civil Engineering
Montana State University, EPS 366, Bozeman, MT 59717

John Sears
Center for Biofilm Engineering and Chemical Engineering
Montana State University, EPS 366, Bozeman, MT 59717

ABSTRACT

The effect of ennoblement on chemistry of passive films on 316L stainless steel (SS) was quantified using surface-sensitive analytical techniques. Under well-defined laboratory conditions, SS coupons were ennobled to ~ +350mV$_{SCE}$ by biofilms of manganese-oxidizing bacterium *Leptothrix discophora* SP-6. Ennobled coupons were analyzed by x-ray photoelectron spectroscopy (XPS) and time-of-flight secondary ion mass spectroscopy (TofSIMS). From the XPS depth profiles of Fe, Cr, O, Ni, C and Mn, we evaluated thickness of the passive layers before and after ennoblement, while the TofSIMS depth profiles were used to evaluate spatial distribution of Mn, Cr, Fe and Ni on the surface. Because the ennobled coupons were covered with biomineralized deposits, sputtering was used to remove these deposits under ultrahigh vacuum (UHV) conditions before probing the chemistry of the underlying passive layers. The main conclusion of the paper is that oxide layers on the ennobled coupons are significantly thinner than those on the pre-ennobled coupons, which may, hypothetically, contribute to their susceptibility to localized corrosion.

Keywords: Ennoblement, manganese-oxidizing bacteria, microbially influenced corrosion, biominerals, passive films, XPS, ESCA, TofSIMS.

* Corresponding author: Zbigniew Lewandowski. E-mail: ZL@erc.montana.edu

INTRODUCTION

Numerous studies have reported increases from -200 mV_{SCE} to +350 mV_{SCE} in the open circuit potentials (OCP) of stainless steels immersed in natural waters; this is known as *ennoblement*. Ennoblement facilitates pitting corrosion in the presence of low amount of aggressive ions, such as Cl^-, which is ordinarily not enough to cause pitting by itself.

Several mechanisms have been proposed for ennoblement: Some models include depolarization of the oxygen reduction reaction caused by enzymes[1,2], strong acidification of the surface from biofilm activity[3,4], combined effects of increased H_2O_2 concentrations and decreased pH from biological origin[5], and reduction of MnO_2 formed by the activity of manganese-oxidizing bacteria. This last mechanism of ennoblement by reduction of biologically produced MnO_2 is the only model that has been proved experimentally in the laboratory as well as in the field[6,7,8,9]. In this model, the reduction of MnO_2 produced by the activity of manganese-oxidizing bacteria (MOB) to MnOOH, reaction (1), and the further reduction of MnOOH to Mn^{2+}, reaction (2), are responsible for the elevated potentials on stainless steel. Reactions (1) and (2) have the same formal electrode potential (E') values as the observed ennoblement potentials in the laboratory and in the field.

$$MnO_2 + H^+ + e^- \rightarrow MnOOH \qquad E' = 383\ mV_{SCE} \qquad (1)$$

$$MnOOH + 3H^+ + e^- \rightarrow Mn^{2+} + H_2O \qquad E' = 336\ mV_{SCE} \qquad (2)$$

Where pH=7.2, $[Mn^{2+}] = 1 \times 10^{-6}$ M.

Pitting corrosion of the turbine runner blades in a hydroelectric power plant has been reported to occur through the activity of manganese-oxidizing bacteria in the presence of a very low chloride concentration which by itself would not be enough to induce the pitting[9]. The results were explained in terms of manganese biomineralization, which was assumed to activate the pitting corrosion by increasing the open circuit potential of the surface. Therefore, it is a possibility that a passive film could be affected by an increased open circuit potential induced by the manganese biomineralization of the surface. The work presented here is based on the assumption that the increase in the OCP caused the changes in the passive film; our goal here is to address whether or not the passive film of a stainless steel surface is affected by manganese biomineralization that gives rise to an increase in the OCP and hence to ennoblement. To achieve this goal, surface-sensitive spectroscopy and imaging tools such as XPS and TofSIMS were used to determine the atomic concentration profiles of Fe, Cr, Ni, O and Mn and elemental images at micron resolution and compare the results with a number of carefully prepared control experiments.

MATERIALS AND METHOD

Ennoblement Experiments

A stock culture of MOB *L. discophora* SP-6 was obtained from American Type Culture Collection (ATCC no. 51168). The organisms were grown in a mineral-salt-pyruvate-vitamin (MSPV) medium (ATCC no. 1917). The composition of the MSVP medium is given in Table 1. The organisms were centrifuged and re-suspended in MSVP medium containing 20% glycerol and preserved in a freezer at –70 °C. These stock cultures were used to inoculate the reactor.

Table 1. ATCC Culture Medium 1917 MSVP for *Leptothrix discophora* SP-6

$(NH_4)_2SO_4$	0.24 g
$MgSO_4.7H_2O$	0.06 g
$CaCl_2.2H_2O$	0.06 g
KH_2PO_4	0.02 g
$Na_2HPO_4.7H_2O$	0.06 g
HEPES	2.383 g
$FeSO_4$ 10 mM	1.0 mL
Distilled water	984 mL

Adjust to pH 7.2 with NaOH or H_2SO_4. Autoclave at 121°C for 15 minutes. Cool to approximately 50°C and aseptically add 1.0 mL of the following filter-sterilized solutions:

20% Sodium pyruvate	
Vitamin solution (see below)	
Biotin	20.0 mg
Folic acid	20.0 mg
Thiamine HCl	50.0 mg
D-(+) -calcium pantothenate	50.0 mg
Vitamin B12	1.0 mg
Riboflavin	50.0 mg
Nicotinic acid	50.0 mg
Pyridoxine HCl	100.0 mg
p-Aminobenzoic acid	50.0 mg
Distilled water to	1.0 L

Type 316L SS coupons 1.6 cm in diameter (composition given in Table 2) were polished as described below, sonicated in acetone, and mounted in polycarbonate holders using a slow-hardening epoxy resin.

Table 2. Composition of 316L stainless steel

Fe	Cr	Ni	Mo	Mn	Si	P	N	C	S
69.34	16.49	10.19	2.10	1.71	0.39	0.034	0.03	0.017	0.001

All the coupons were polished using 240, 360, 400 and 600 grit size sandpapers followed by fine polishing with 5.0-, 0.3-, and 0.05-micron Al_2O_3 particles placed on microcloths. Following the mounting on the polycarbonate coupon holders, the electrical connections were made by attaching a copper wire to the back of each coupon. The contact resistances of the coupons were measured to make sure that the values were less than 1 ohm. The coupons were sterilized in ethyl alcohol solution under the biohood for three hours. The coupons (up to 6 coupons) were then placed into the autoclaved polycarbonate 500 mL-reactor containing MSVP medium excluding $FeSO_4$ ($FeSO_4$ is only used in stock culture preparations). Manganese was added as $MnSO_4$ (0.2 mM) using a sterile syringe filter. Potentials were measured hourly by a data acquisition system against a saturated calomel electrode (SCE). After 6-7 days, the OCP reaches a stable reading ~+350 mV_{SCE}, the coupons were removed for surface analysis. At this time the coupons are considered ennobled and are removed from the reactor and taken for analysis immediately.

The XPS and TofSIMS experiments were conducted on the five groups of coupons, four of which served as controls. The first group of coupons was subjected to a series of MOB-induced ennoblement processes as described above. One of the four groups of control coupons was as-received coupons subjected only to the polishing and cleaning procedure described above. The second group of control coupons was immersed into pure sterile water for the same period of time as the other control coupons. The XPS and TofSIMS experiments conducted on the two groups of coupons described above serve as the background measurements with respect to which other results were compared. The third group of control coupons was treated with sterile MSVP and a 0.2 mM Mn^{2+} solution without any bacteria (herein termed *growth medium treated* coupon) in order to determine the effect, if any, of the growth medium on the stainless steel passive film. The fourth group of control coupons was exposed to MSVP and the bacteria solution without any Mn^{2+} (called *biofilm treated coupons*) in order to determine the effect of bacteria on the passive film without the Mn^{2+} ions in the medium. Prior to XPS and TofSIMS analysis, coupons were wiped or rinsed, as explained below in detail, and then the coupons were removed from the polycarbonate holders mechanically, making sure that no epoxy was left on back of the coupons before inserting them in the UHV chamber.

XPS Analysis

XPS experiments were performed using a PHI Model 5600ci MultiTechnique system. A monochromatized Al K alpha (1486.6 eV) x-ray source was used. An 800-micron diameter equivalent area of the sample surface was analyzed while a 3x3-mm^2 area was sputtered using Ar^+ ions for each cycle of depth profiling. In the sputtering process, Ar^+ ions, accelerated to ~ 2 keV at 0.25 μA current, were used to bombard the sample surface for selected time intervals (~0.5 min) until Fe and Cr oxides were removed and metallic Fe and Cr (bulk SS) were reached. Following each cycle of sputtering, multiplex XPS spectra of selected core level emissions were taken to determine the depth profiles of Mn, Fe, C, O and Ni for each of the controls and the ennobled coupons. Ni depth profile was omitted in the figures because of low Ni concentration in the passive film and because no variation with any treatment was observed in the Ni profile.

TofSIMS Experiments

A Phi-Evan's Trift-I system was used for the TofSIMS experiments; this consists of a liquid metal (Ga^+) ion gun for obtaining high mass and high spatial resolutions for chemical imaging. In these experiments 25 keV Ga^+ primary ions were used to generate secondary ions. These ions are separated and detected by a triple-pass 90° spherical sector electrostatic mass analyzer. The output is a high-resolution mass spectrum plotted as a function of intensity vs. mass-to-charge ratio. For chemical maps a 256x256 pixel area (typically corresponding to a 120x120 square micron size) with each pixel containing the full mass spectrum was stored in the computer media as raw files. Chemical maps of Fe, Cr and Mn (Ni was omitted for the same reason as explained above) were extracted retrospectively following the raw data acquisition.

RESULTS AND DISCUSSION

XPS Analysis

XPS analysis was conducted on samples prepared in two different ways: (1) coupon surfaces were rinsed with pure water and wiped completely with a cotton swab to remove the biomineral deposits, and (2) coupon surfaces were rinsed gently with pure water only, leaving the biomineral deposits on the surface. At least two different areas were analyzed on a given coupon. The motivation for removing the biofilms before analysis (preparation 1) is to determine whether or not substantial changes are introduced to the passive layer as a result of biofilm activity. Such a change usually manifests itself with increased passive layer thickness as compared with the controls[12]. The motivation for leaving the biofilm intact (preparation 2) is to prevent repassivation in case the ennoblement reduces the film thickness and compromises the passive film in such a way that removal of biominerals and exposure to ambient conditions will simply cause the re-oxidation of the surface before one can determine the changes due to ennoblement. It is likely that if the biofilm is left on the surface re-oxidation of the passive layer in air will be prevented and a depth profile analysis conducted in the UHV environment will reveal the reduction in the passive layer thickness as a result of the ennoblement. The data presented below support the latter prediction.

Stainless steel coupons with removed biomineral deposits: Each data point in the depth profile graph is generated by quantitative analysis of the individual core-level spectra acquired during each cycle of depth profiling. In Figs. 1-3 we show the XPS depth profiles corresponding to the ennobled and control coupons whose surfaces were completely cleaned by rinsing with pure water and wiping with cotton swabs. The depth profiles for the as-received and pure water treated coupons look identical to those shown in Figs. 1-3 and hence are not shown here. The passive film thicknesses of those coupons, however, are listed in Table 3.

Stainless steel coupons with intact biomineral deposits: The depth profiles of O, C, Fe, and Cr of the coupons subjected to biofilms of *L. discophora* without introducing Mn^{2+} into the solution and without removal of biofilm are given in Fig. 4. These coupons were not ennobled, because of a lack of Mn^{2+} ions. The depth profiles of the same elements for the coupons which are ennobled because of biofilm and Mn activity without removal of biomineral deposits are given in Fig. 5.

The depth profiles shown in Fig. 1 for the control coupons (growth medium treated coupons) show two regions of interest; (1) an O- and Cr-rich region and (2) a metallic Fe- and Cr-rich (bulk SS) region. The Cr profile shows a maximum in the first region (Fig. 1). As expected, the O concentration decreases while the Fe concentration increases to its bulk value as a function of sputter depth. Other researchers[10,11] have also reported the existence of Cr-rich regions in passive films. No Ni-oxides were detected in the passive films (results were not presented), which is also in agreement with the literature[11,12,13].

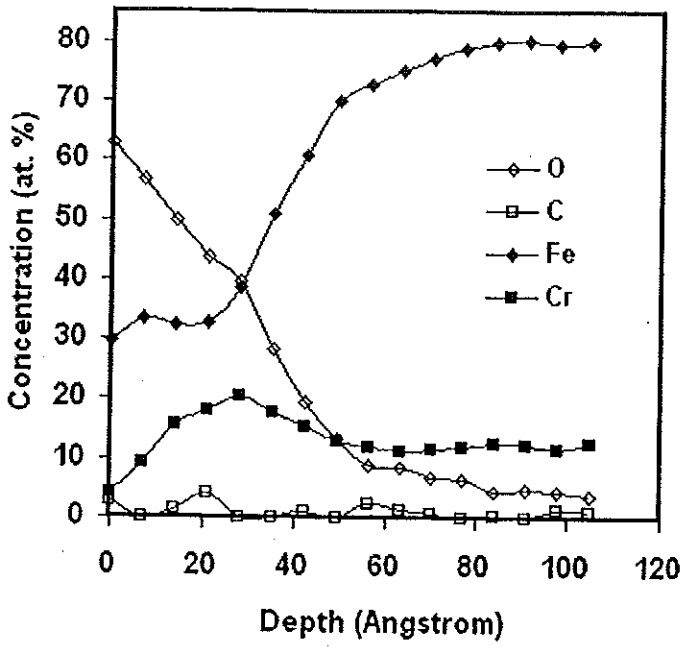

Figure 1. Depth profiles of O, C, Fe and Cr for the growth medium treated control coupon.

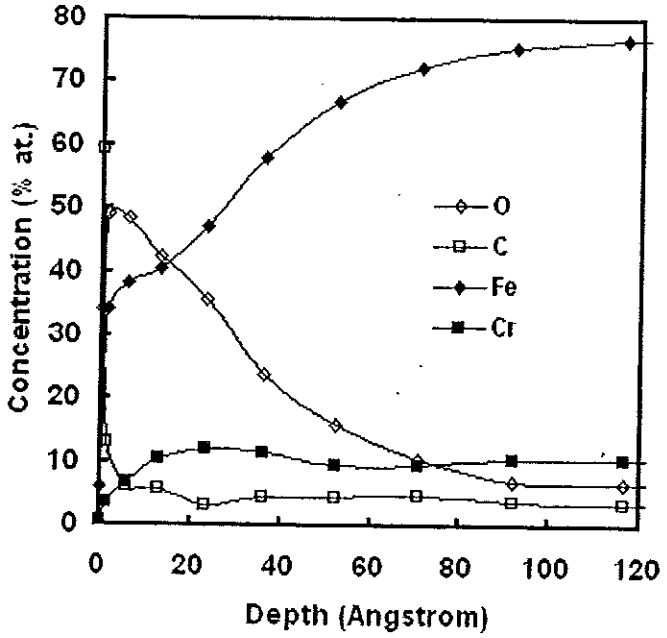

Figure 2. Depth profiles of O, C, Fe and Cr for the *L. discophora* biofilm treated control coupon following complete removal of biofilm.

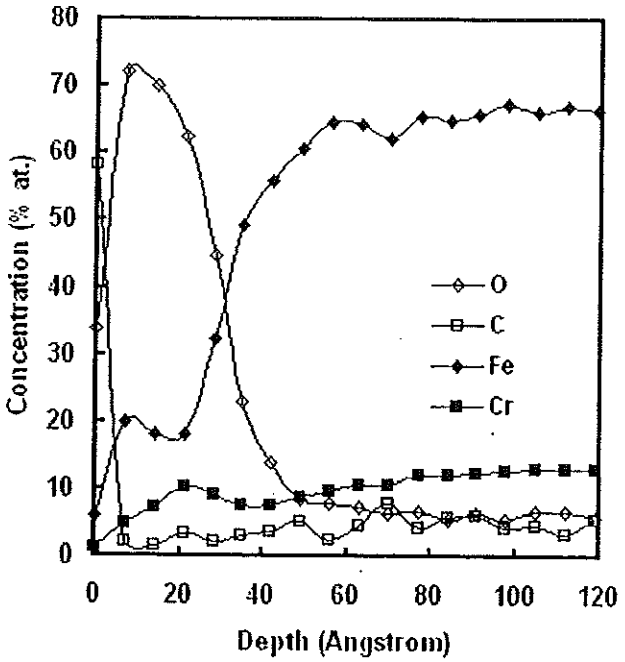

Figure 3. Depth profiles of O, C, Fe and Cr for the ennobled coupon after removal of biomineral deposits. Notice that the passive layer thickness appears to remain the same as that of the control coupons. This is explained in terms of re-oxidation of the surface (see text).

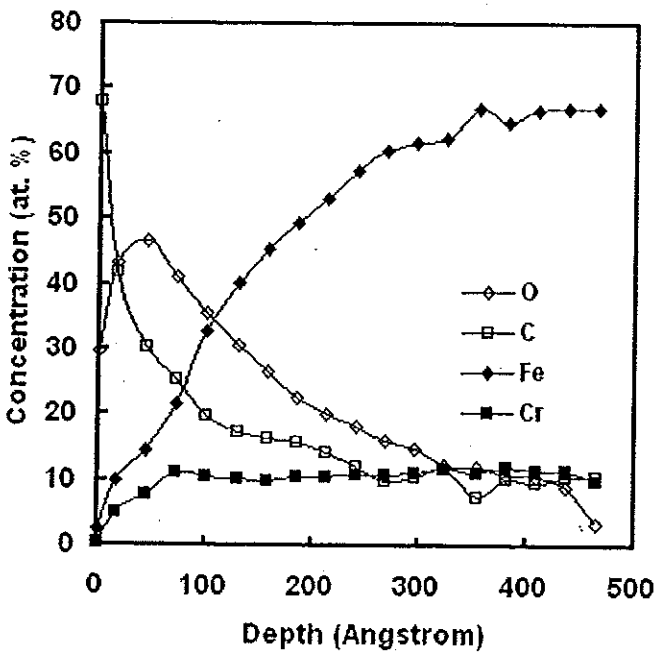

Figure 4. Depth profiles of O, C, Fe and Cr *for the L. discophora* biofilm treated coupon without the removal of biominerals.

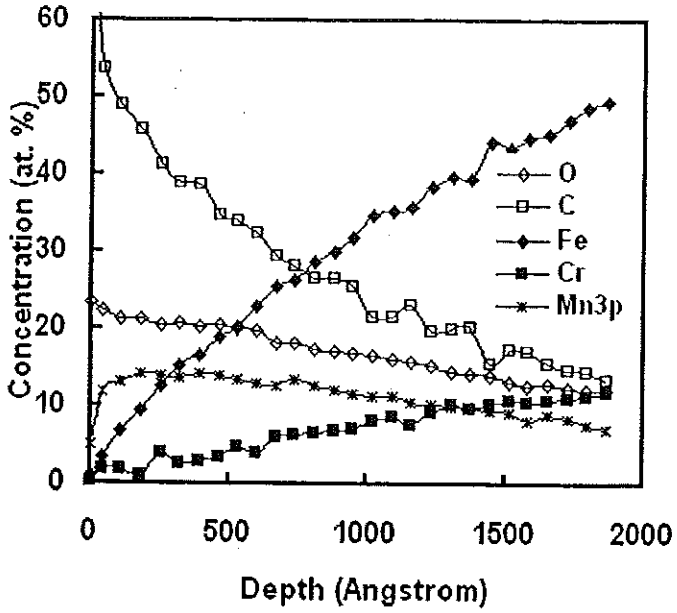

Figure 5. Depth profiles of O, C, Fe and Cr for the ennobled coupon without the removal of biomineral deposits.

In order to plot the depth profiles of the Fe-oxide and Cr-oxide layers, the Fe $2p_{3/2}$ and Cr $2p_{3/2}$ peaks after each sputtering cycle were separated into the oxide and bulk metallic components. This is because Fe $2p_{3/2}$ and Cr $2p_{3/2}$ have two contributions, one from the oxidized portion of the passive film and the other from the metallic portion (bulk SS) under the passive layer. The XPS curve fits were made to separate the oxide and bulk contributions to the Fe $2p_{3/2}$ and Cr $2p_{3/2}$ peaks as shown in Figs. 6 and 7. Metallic Fe has a peak centered at ~707.6 eV, and the metallic Cr has a peak at 574.3 eV. The areas under the metallic component and the rest of the total peak determine the relative concentrations of the two contributions. The data points shown in Figs. 8-12 corresponding to Fe and Fe-oxide and Cr and Cr-oxide depth profiles, respectively, were obtained from the areas associated with the metallic and oxide contributions. The position and the full-width-at-half-maximum (FWHM) of the metallic component are determined using the control coupons by sputtering them until the passive layer is totally removed. The resultant Fe and Cr peaks are used as standards: The position and FWHM of these peaks are used for fitting the composite peaks as in Figs. 6 and 7, by adjusting the intensity for the best fit to determine the bulk and oxide contributions. The bulk contribution was subtracted from the total area under the $2p_{3/2}$ peak to determine the oxide contributions that in general consist of multiple oxide peaks. In Figs. 8-12 we show Fe and Fe-oxides and Cr and Cr-oxides profiles for various samples we have studied. The thickness determination and sputter rate were done by referencing to a SiO_2 standard, which using our rate of sputtering resulted in ~ 7 Å/min.

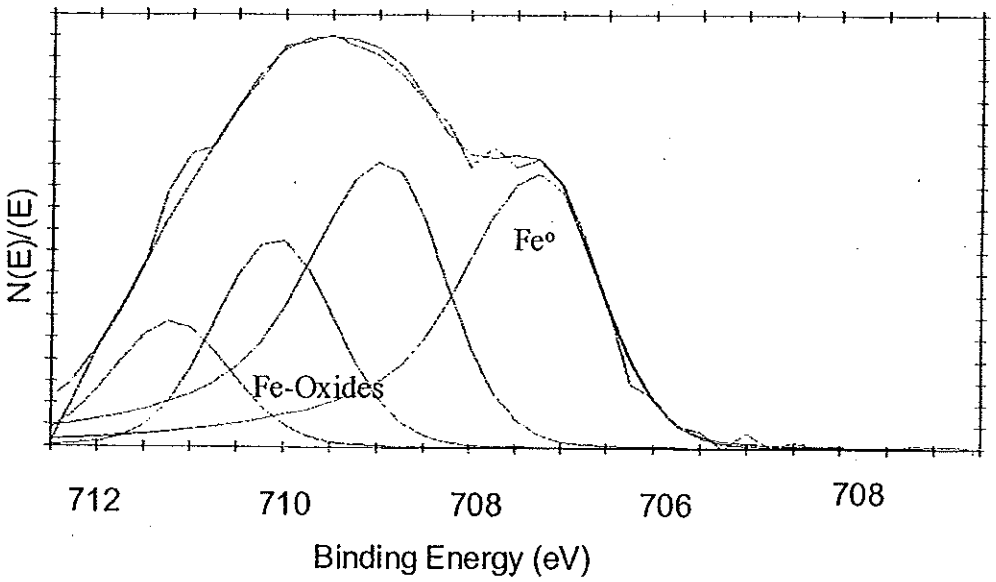

Figure 6. XPS curve fit for the Fe $2_{p3/2}$ profile to determine the bulk and oxide contributions.

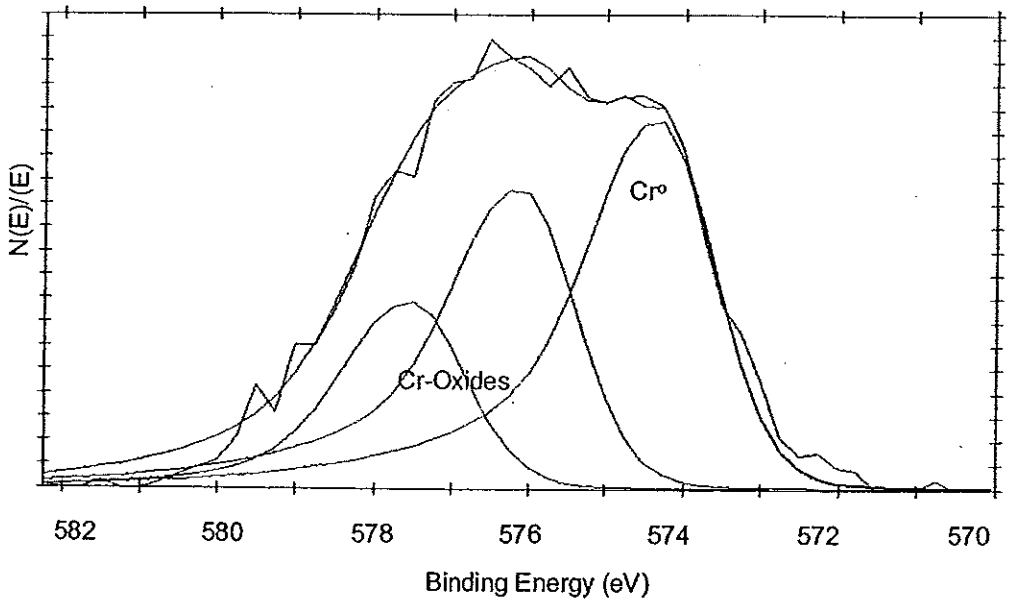

Figure 7. XPS curve fit for the Cr $2_{p3/2}$ profile to separate the oxide and bulk contributions.

Before the passive layer under the biofilm can be analyzed, we need to sputter-clean the thick biofilm deposits in UHV. This is shown in Fig. 5, which gives the depth profile of an ennobled coupon containing biomineral deposits. Notice that the total Fe concentration increases linearly during sputtering, up to 2000 Angstrom, without leveling off. Since most of the O is from biominerals, which cover a large fraction of the area, it levels off at values indicating that a substantial fraction of the area is covered by biominerals. We interpret the linear increase in the Fe concentration (Fig. 5) in terms of

exposing new areas of the passive layer. This is because the biomineral deposits will form variable thicknesses across the surface, so that as the surface is sputtered the portions having thin film deposits will be removed and the passive layer will be exposed and will contribute to both Fe and Cr concentrations. It is these areas that we are very interested in analyzing. If the thickness of the passive layer has not changed each time a fresh area is exposed, it is expected that oxidized Fe and Cr regions will be recovered. Ideally this should show an *apparent increase* in the oxide thickness, though in reality we are exposing new areas under the biofilm. In our observations we do not see the *apparent increase* in the oxide thickness (see Fig. 12 a,b). This we interpret as the passive layer thickness decreasing so that we can not resolve the metal oxides at each sputter cycle in the passive layer, though we can register the metallic components as we expose the passive layer.

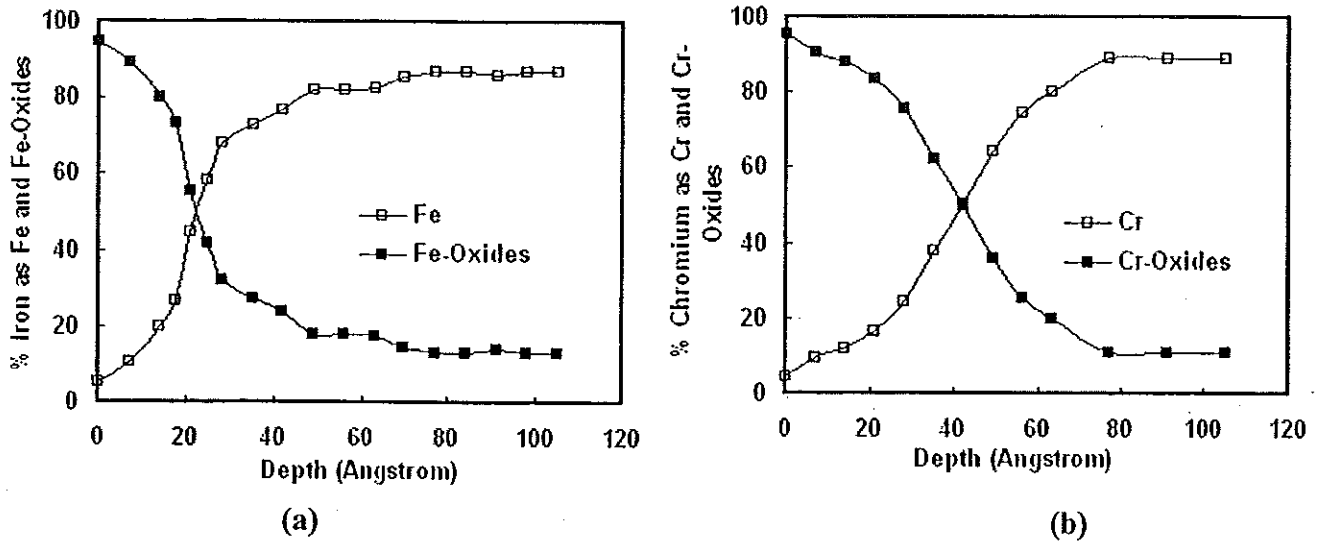

Figure 8 a) Fe and Fe-oxides **b)** Cr and Cr-oxides depth profiles for growth medium treated coupon

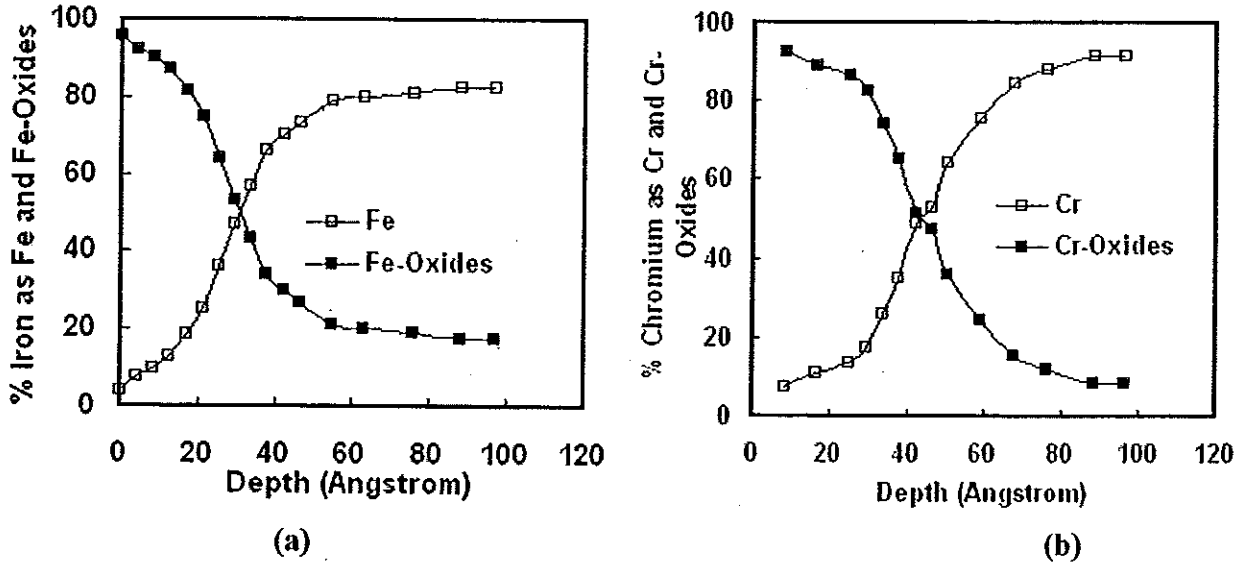

Figure 9 a) Fe and Fe-oxides **b)** Cr and Cr-oxides depth profiles for *L. discophora* biofilm treated coupon after removal of biominerals.

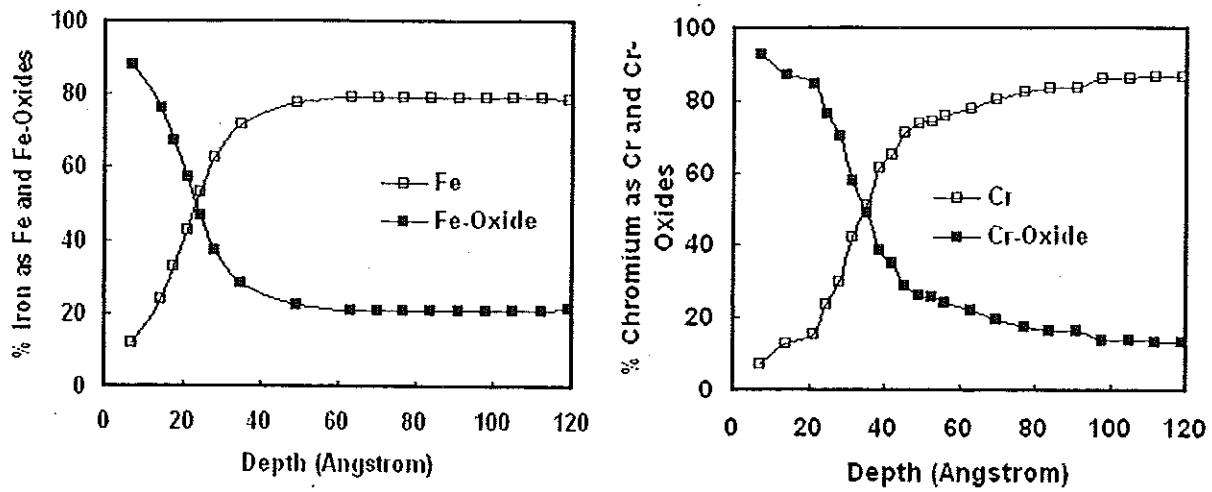

(a) (b)

Figure 10 a) Fe and Fe-oxides **b)** Cr and Cr-oxides depth profiles for ennobled coupon after removal of biomineral deposits.

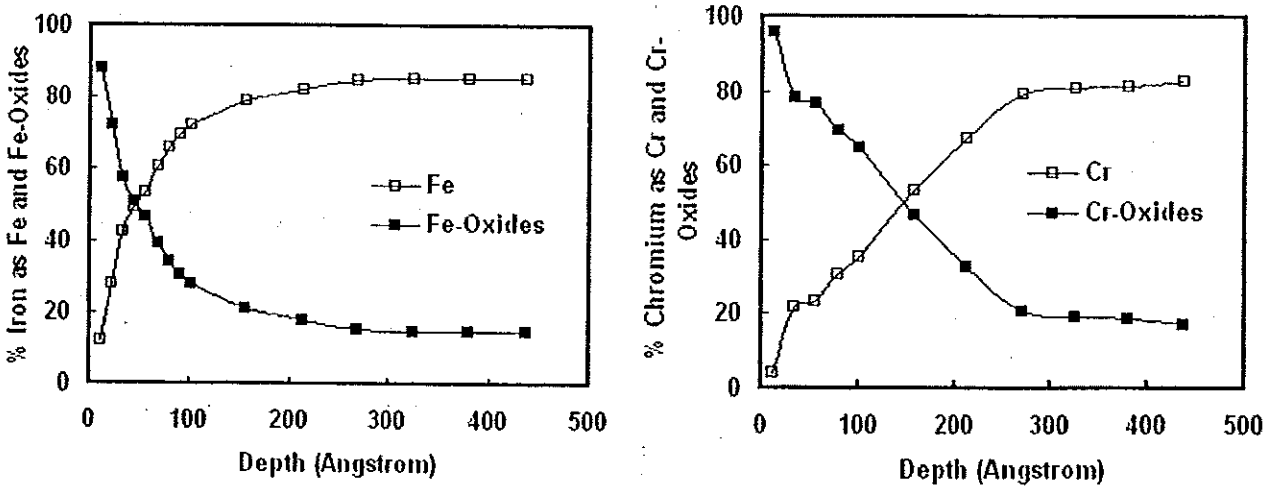

(a) (b)

Figure 11 a) Fe and Fe-oxides **b)** Cr and Cr-oxides depth profiles for *L. discophora* biofilm treated coupons (without Mn^{2+}; no ennoblement) without removal of biofilm.

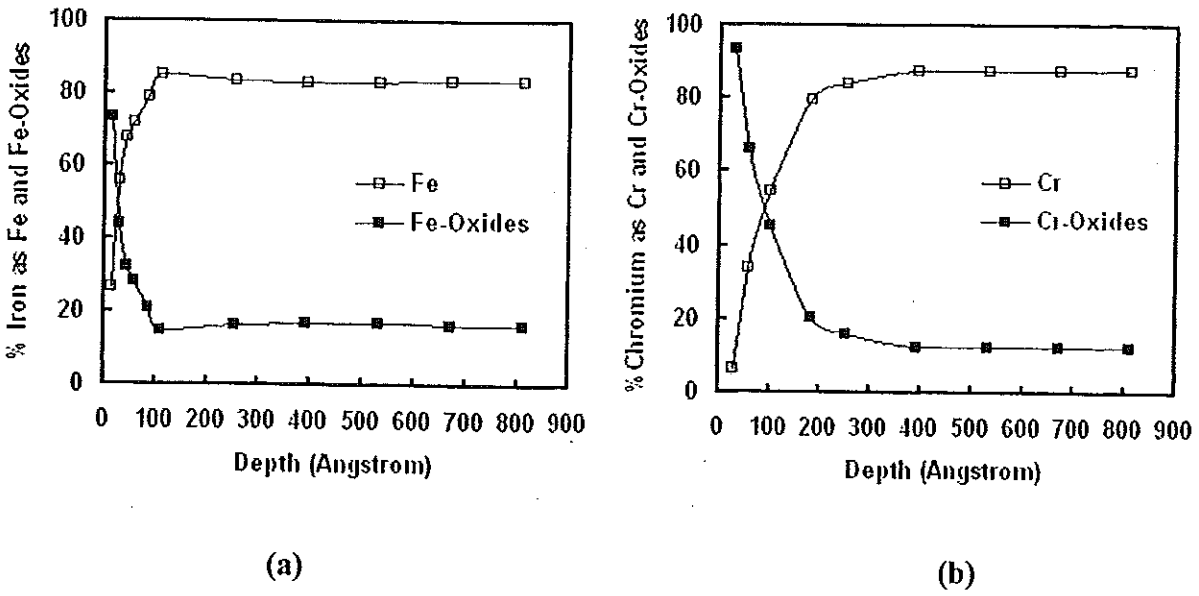

Figure 12 a) Fe and Fe-oxides **b)** Cr and Cr-oxides depth profiles for ennobled coupon without removal of the biomineral deposits.

The thicknesses of the Fe-oxide and Cr-oxide layers on coupons after the removal of Mn-rich biominerals can be determined by making use of Figs. 8-12. The depth of the appropriate oxide was determined from the value at which the metallic contribution becomes constant. The data suggest that the Fe-oxide layer was sputtered before the Cr-oxide layer. This proves that the passive film is composed of a Fe-rich outer layer and a Cr-rich inner layer. This duplex characteristic of stainless steel passive film has been confirmed by other researchers[14,15,16,17,18].

The film thicknesses for the Fe-oxide layer and the Cr-oxide layer on the coupons after removal of biomineral deposits are summarized in Table 3. The results show no significant difference among the coupons. As discussed earlier, the possibility of repassivation makes it impossible to differentiate the actual film thicknesses of the ennobled coupons. We have no easy way to carry out the XPS depth-profiling analysis by removing biomineral deposits from the surface without causing repassivation, except for keeping the biomineral deposits on the coupon and sputtering them off in the UHV environment. The results of such an analysis of ennobled coupons were rather surprising, as seen in Fig. 12 (a,b) corresponding to the Fe and Fe-oxide and Cr and Cr-oxide profiles. Even though the Fe atomic concentration increases linearly (Fig. 5) with sputtering cycle, which was interpreted as the sputtering process removing the thin portions of the bio-deposits and opening up new areas under the passive films, we do not observe the expected *apparent increase* in the passive layer thickness. This increase in the apparent thickness is expected because, considering that the rate of sputtering is about ~3-5 Å per cycle, it would be impossible to miss the passive layer by oversputtering unless the passive layer thickness under the biofilm of the ennobled coupon were reduced, perhaps down to 5-10 Å! This hypothesis is reinforced by the observation that if the Fe and Fe-oxide and Cr and Cr-oxide profiles shown in Fig. 12 (a,b) (ennobled coupons) are compared with the control coupon profiles shown in Fig. 11 (a,b) (biofilm treated coupon) the *apparent increase* in the passive layer is observed as anticipated provided that the thin film under the biofilm is not compromised. If the depth profiles of Fig. 11 (a,b) are conducted following the removal of the biofilm, as shown if Fig. 10 (a,b), no change in the passive layer

is observed. We conclude, therefore, that the ennoblement of a coupon under the influence of MOB and the reduction of the passive layer thickness appear to be correlated.

Table 3. Passive film thicknesses in Angstrom for the coupons after removal of biofilm/-Mn-deposits.

	As-received polished	Pure water treated	Growth medium treated	Biofilm treated	Ennobled
Fe-Oxide	30	40	50	60	40
Cr-Oxide	35	70	70	80	80

TofSIMS Results

To elucidate the nature the chemical processes that cause the reduction of the passive layer we investigated whether or not there is material dissolution in the passive layer. Taking advantage of the imaging capabilities and high sensitivities of TofSIMS we carried out depth profile investigations on ennobled coupon surfaces. Figures 13 and 14 show the TofSIMS images of Mn^+, Cr^+ and FeH^+ ions for the ennobled coupons at 420 and 2600-Angstrom depths respectively (referenced to the depth measurements conducted on Si-wafers). The dimension of each image is ~ 60x60 microns. The white spots show high concentrations of related element.

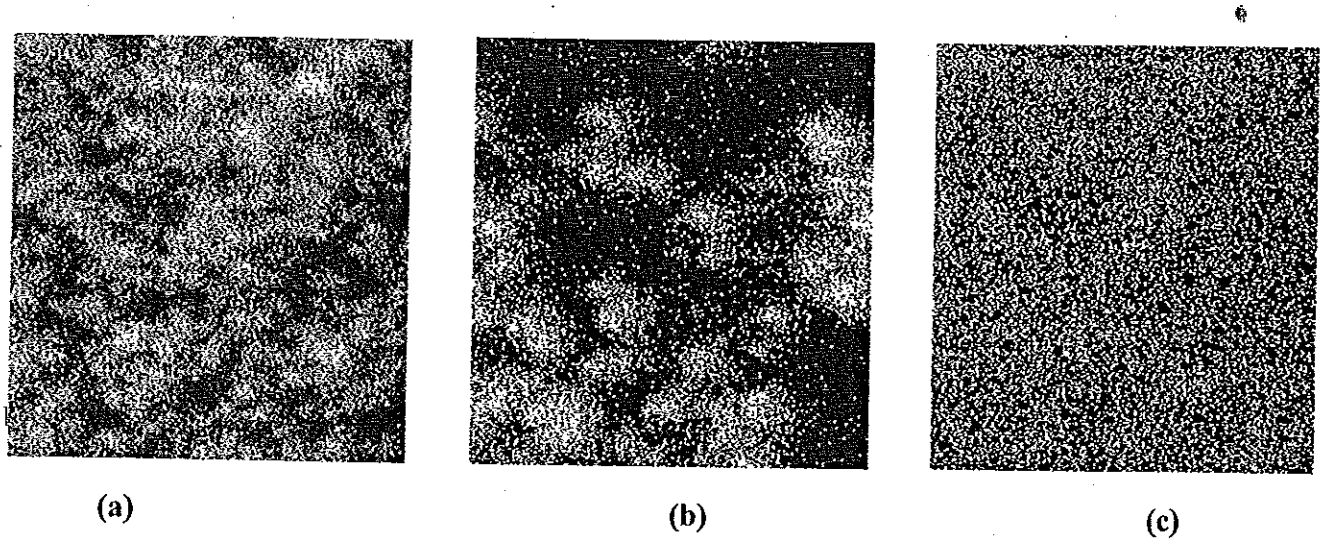

(a) (b) (c)

Figure 13. TofSIMS images of (a) Mn^+, (b) Cr^+ and (c) FeH^+ for an ennobled coupon at 420-Angstrom depth.

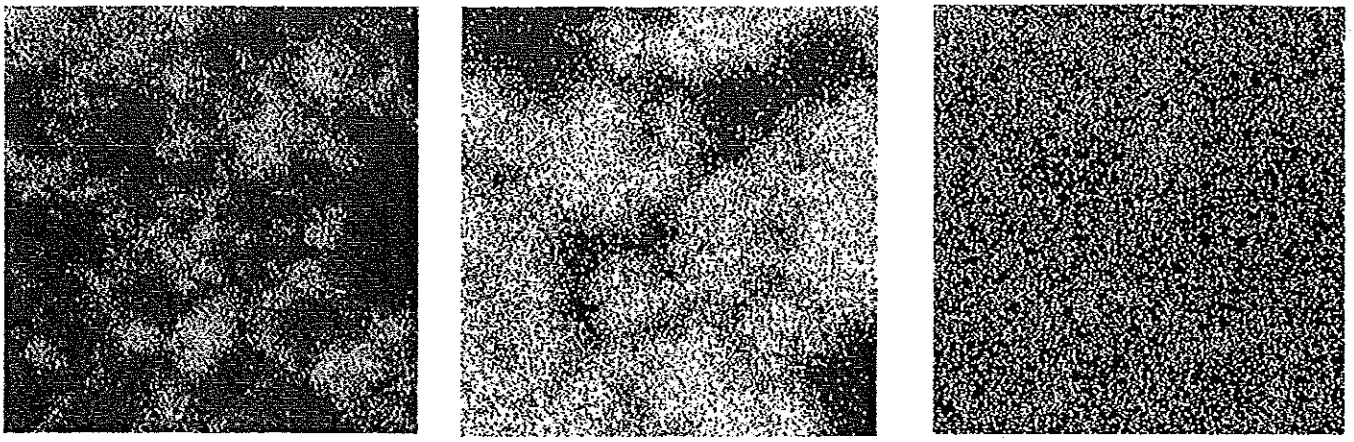

(a) (b) (c)

Figure 14. TofSIMS images of (a) Mn^+, (b) Cr^+ and (c) FeH^+ for an ennobled coupon at 2600-Angstrom depth.

The decrease in Mn and increase in Cr images at higher depths show that the sputtering process removes some of the manganese deposits and opens up fresh metallic surface. When Mn and Cr images from given depths are compared, it is clear that the two elemental images are complementary in that Cr is present where minimal or no Mn is present. This means Cr originates from the passive layers or bulk of the stainless steel surface. However, the Fe images (as represented by FeH^+ rather than Fe^+ to prevent confusion with MnH^+) indicate that Fe is present both mixed with the Mn deposits inside the biofilm and on bare SS surface. Since the concentration of total Fe in the treatment solution was below 0.005 ppm before treatment and 0.009 ppm after treatment, the observation of Fe in the biofilm is interpreted as Fe dissolving from the passive film and mixing into the biomineral deposits. A region-of-interest TofSIMS analysis of Cr-rich and Mn-rich areas shows no Cr in the black areas (Mn-rich areas) but shows proper concentrations of Cr, Ni and Fe in bright areas (bulk SS) from the clean stainless steel surface, as expected.

CONCLUSIONS

The biomineral-deposits on the stainless steel surface that cause ennoblement also cause degradation of the passive film on the surface in such a way that the passive film thickness is reduced. A possible mechanism of degradation can be related to Fe dissolution into the biofilm matrix. The two processes perhaps are linked by the oxidation reactions that involve manganese.

AKNOWLEDGEMENTS

The research was supported by United States Office of Naval Research contract number N00014-99-1-0701 and by cooperative agreement EED-8907039 between the National Science Foundation and Montana State University. The authors would like to thank Xianming Shi for his help with the TofSIMS analysis. The authors would like to thank the Image and Chemical Analysis Laboratory personnel for their help during TofSIMS and XPS experiments.

REFERENCES

1. V. R. Scotto, R. DiCintio, G. Marcenaro, Corrosion Science 25 (1985): p.185.

2. A. Mollica, International Biodeterioration and Biodegradation 29 (1990): p. 213.

3. B. Little, R. Wagner, Z. Lewandowski, W.C. Lee, W. G. Characklis, W. F. Mansfeld, in corrosion/90, paper no. 90150 (Houston, TX: NACE International, 1990).
Z. Lewandowski, W.C. Lee, W. G. Characklis, B. Little in Corrosion/89, paper no. 93 (Houston, TX: NACE International, 1989).

4. P. Chandrasekaran, S.C. Dexter, in Proceedings of 12th International Corrosion Congress, 5B, 3696-3703, 1993.

5. D. Feron, I. Dupont, G. Novel, European Federation of Corrosion, No.22, ed. The Institute of Materials Editor, 103-112, 1997.

6. W. H. Dickinson, Z. Lewandowski, Biofouling 10 (1-3)(1996): p. 79.

7. W. H. Dickinson, F. Caccavo Jr., Z. Lewandowski, Corrosion Science, 38(1996): p. 1407.

8. B. H. Olesen, R. Avci, Z. Lewandowski, Corrosion Science, 42 (2000): p. 211.

9. P. Linhardt, "Failure of Chromium-Nickel Steel in a Hydroelectric Power Plant by Managanese-Oxidizing Bacteria" in Microbially Influenced Corrosion of Materials, eds Heitz et al. Springer-Verlag Berlin Heidelberg, 1996, p. 221.

10. G. Lorang, M. Da Cunha Belo, A. M. Simoes, M. G. S. Ferrerira, J. Electrochem. Soc., 141 (1994): p. 3347.

11. P. Jyostna, Ph.D. Thesis, Department of Physics at Montana State University (1996).

12. I. Olefjord, B. Brox, U. Jelvestam, J. Electrochem. Soc.: ELECTROCHEMICAL SCIENCE AND TECHNOLOGY, 132 (1985): p. 2854.

13. C. R. Clayton and Y. C. Lu, J. Electrochem. Soc.: ELECTROCHEMICAL SCIENCE AND TECHNOLOGY 133, 12(1986): p. 2465.

14. A. R. Brooks, C. R. Clayton, K. Doss, Y.C. Lu, J. Electrochem. Soc.: ELECTROCHEMICAL SCIENCE AND TECHNOLOGY, 133 (1986): p. 2459.

15. G. M. Lorang, M. Da Cunha Belo, J. P. Langeron, J. Vac. Sci. Technol. A5 (1987): p. 1213.

16. G. Lorang, F. Basile, M. Da Cunha Belo, J. P. Langeron, Surf. Interface Anal. 12 (1988): p. 424.

17. N. E. Hakiki, S. Boudin, B. Rondot, M. Da Cunha Belo, Corrosion Science, 37 (1995): p.1809.

18. M. Da Cunha Belo, B. Rondot, C. Compere, M.F. Montemor, A.M.P. Simoes, M.G.S. Ferreira, Corrosion Science, 40 (1998): p. 481.